ACS Catalysis

Research Article

pubs.acs.org/acscatalysis

Multiproduct Steady-State Isotopic Transient Kinetic Analysis of the Ethanol Coupling Reaction over Hydroxyapatite and Magnesia

Sabra Hanspal, Zachary D. Young, Heng Shou,† and Robert J. Davis*

Department of Chemical Engineering, University of Virginia, 102 Engineers' Way, Charlottesville, Virginia 22904-4741, United States

Supporting Information

ABSTRACT: The Guerbet coupling of ethanol into butanol was investigated using multiproduct steady-state isotopic transient kinetic analysis (SSITKA) in a comparative study between stoichiometric hydroxyapatite (HAP) and magnesia (MgO) catalysts at 613 and 653 K, respectively. The steady-state catalytic reactions were conducted in a gas-phase, fixed-bed, differential reactor at 1.3 atm total system pressure. Multiproduct SSITKA results showed that the mean surface residence time of reactive intermediates leading to acetaldehyde was significantly shorter than that of intermediates leading to butanol on both HAP and MgO. This finding may suggest that the dehydrogenation of ethanol to acetaldehyde is fast on these surfaces compared with C−C bond formation. If adsorbed acetaldehyde is a key reaction intermediate in the Guerbet coupling of ethanol into butanol, then SSITKA revealed that the majority of adsorbed acetaldehyde produced on the surface of MgO desorbs into the gas-phase, whereas the majority of adsorbed acetaldehyde on HAP likely undergoes sequential aldol-type reactions required for butanol formation. Adsorption microcalorimetry of triethylamine and CO_2 showed a significantly higher number of acid and base sites on the surface of HAP compared with those on MgO. Diffuse reflectance infrared Fourier transform spectroscopy of adsorbed ethanol followed by stepwise temperature-programmed desorption revealed that ethoxide is more weakly bound to the HAP surface compared with MgO. A high surface density of acid−base site pairs along with a weak binding affinity for ethanol on HAP may provide a possible explanation for the increased activity and high butanol selectivity observed with HAP compared with MgO catalysts in the ethanol coupling reaction.

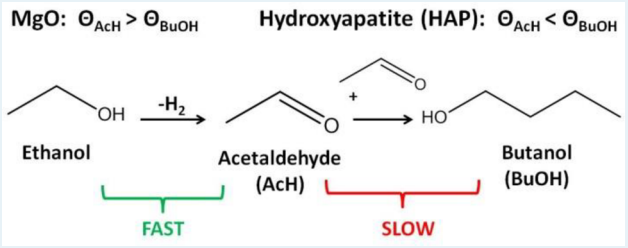

KEYWORDS: *hydroxyapatite, magnesia, Guerbet reaction, ethanol, butanol, microcalorimetry, DRIFTS, steady-state isotopic transient kinetic analysis (SSITKA), acid−base bifunctional catalyst*

1. INTRODUCTION

The use of corn-based bioethanol as a domestic and renewable transportation fuel alternative has led to a growth of ethanol production in the United States. This increased availability combined with several drawbacks posed by ethanol as a blend fuel has called attention to its catalytic transformation into a higher-value fuel or chemical such as butanol.[1] Butanol is an important industrial chemical and has recently generated interest as a potential gasoline fuel additive due to its higher energy density relative to ethanol and, thus, ability to improve fuel economy for biofuel blended gasoline.[1,2]

Butanol is commonly synthesized by hydroformylation via the oxo process. This method uses fossil fuel-derived feedstocks and often requires expensive catalytic materials and extreme reaction pressures, leading to high energy input and substantial operating costs.[3,4] An alternative route to butanol synthesis is the catalytic conversion of bioderived ethanol via the so-called Guerbet reaction.

The Guerbet reaction is a well-known industrial route for higher alcohol synthesis that ultimately couples two short-chain alcohols to produce a longer-chain saturated alcohol. The most commonly accepted reaction sequence for the Guerbet coupling of ethanol involves an initial dehydrogenation step to form acetaldehyde, which then undergoes an aldol condensation reaction, followed by hydrogenation of the resulting unsaturated condensation products to give butanol.[5−7]

Alternative reaction pathways for ethanol coupling have been proposed by researchers in the field, primarily those involving a "direct" condensation route without the participation of gas-phase acetaldehyde.[3,8−11] This "direct" bimolecular path was verified by Iglesia and co-workers through studies of ^{13}C-labeled acetaldehyde reacting with ethanol over K−Cu/$MgCeO_x$ catalysts at short contact times, which resulted in a portion of the coupled products being unlabeled, suggesting that ethanol coupling can proceed without the presence of gas-phase acetaldehyde.[10] Recently, Scalbert et al.[11] investigated the role of acetaldehyde self-aldolization in the ethanol coupling reaction over a hydroxyapatite catalyst using a thermodynamic approach and also found that the reaction primarily proceeds through a "direct" biomolecular route and that aldol condensation of acetaldehyde is a minor pathway in the sequence leading to butanol. The details regarding the "direct"

Received: December 16, 2014
Revised: February 2, 2015
Published: February 4, 2015

DOI: 10.1021/cs502023g
ACS Catal. 2015, 5, 1737−1746

condensation route, as to whether the reaction mechanism involves the direct self-coupling of two ethanol molecules or the condensation of ethanol and acetaldehyde, remain unclear, and therefore, mechanistic studies are still ongoing. For a more comprehensive discussion of Guerbet chemistry, including details regarding the reaction mechanism, please refer to the recent review paper by Kozlowski and Davis.[12]

The ethanol coupling reaction has been extensively studied over a wide range of catalytic materials, such as solid base metal oxides,[13,14] both unpromoted and modified by transition metal or alkaline earth metal components;[9,10] hydrotalcite-derived Mg−Al mixed oxides;[15,16] and alkali metal ion-exchanged zeolites.[8,17] These catalysts typically require high reaction temperatures (>673 K) and produce butanol with poor selectivities at relatively low rates. Recent studies have demonstrated unusually high activity and high butanol selectivity for the Guerbet coupling of ethanol over hydroxyapatite catalysts.[18,19]

The stoichiometric form of hydroxyapatite (HAP, $Ca_{10}(PO_4)_6(OH)_2$) has a Ca/P molar ratio equal to 1.67; however, this ratio can vary substantially in synthetic materials. The surfaces of HAP can be acidic or basic in nature, depending on the Ca/P molar ratio of the material, which in turn influences the catalytic behavior of HAP.[20−22] The active sites on these materials have not been identified, and therefore, a detailed understanding of the reaction mechanism is lacking. In this study, we used steady-state isotopic transient kinetic analysis (SSITKA) of the ethanol coupling reaction over a stoichiometric calcium hydroxyapatite catalyst and compared the results with those obtained with MgO, a standard solid base catalyst, in an effort to gain insight into the reaction mechanism at the active site level.

The SSITKA technique is a well-established and powerful method that allows quantification of important kinetic parameters, such as surface coverages of adsorbed reactant species and surface reaction intermediates, average surface lifetimes of those intermediates, and an upper bound of the turnover frequency.[23−25] For additional details regarding the SSITKA technique, see the comprehensive review by Shannon and Goodwin.[26] Recently, our group studied the gas-phase conversion of ethanol to butanol over MgO at 673 K using SSITKA; however, acetaldehyde could not be followed as an intermediate with the reaction system.[27] In the present work, we have performed a comparative study between stoichiometric hydroxyapatite (HAP) and MgO, using a modified SSITKA reactor system that allows the monitoring of multiple products formed during the reaction.

To relate reactivity results to catalyst properties, adsorption sites on the catalysts were characterized using diffuse reflectance FT-IR spectroscopy (DRIFTS) during stepwise temperature-programmed desorption (STPD) of adsorbed ethanol as well as adsorption microcalorimetry of carbon dioxide, triethylamine, and ethanol. Results from surface characterization, reactivity testing, and isotopic transient studies were used to propose key structural and compositional properties that facilitate the Guerbet coupling reaction.

2. EXPERIMENTAL METHODS

2.1. Catalyst Preparation. The calcium hydroxyapatite catalyst was prepared using a controlled coprecipitation method based on the procedure described by Tsuchida et al.[28] First, two aqueous solutions were prepared: 200 cm^3 of 0.5 M calcium nitrate tetrahydrate ($Ca(NO_3)_2{\cdot}4H_2O$, Acros Organics) and 200 cm^3 of 0.3 M diammonium phosphate ($(NH_4)_2HPO_4$, Aldrich, >99.99%). These compositions corresponded to a stoichiometric molar ratio of Ca/P (1.67) in the resulting mixed solution. Both solutions, previously adjusted with aqueous ammonia to pH = 10.5, were simultaneously added dropwise to 100 cm^3 of distilled deionized water (DDI) at 353 K. Sufficient aqueous ammonia was added continuously during precipitation to maintain a pH of 10.5. The resulting suspension was stirred for 24 h at 353 K. The precipitate was recovered by vacuum filtration, washed 3 times with DDI water, and dried in air at 400 K overnight.

High-purity and ultrafine (500 Å) MgO was obtained commercially (Ube Material Industries, Ltd.). The MgO and HAP powders were calcined at 873 K for 2 h in flowing air using a 10 K min^{-1} ramp rate, then pressed, crushed, and sieved into pellets of 106−180 μm.

2.2. Catalyst Characterization. Crystalline phases of the catalysts were confirmed by powder X-ray diffraction (XRD) on a PANalytical X'Pert Pro diffractometer using monochromatic Cu Kα radiation (λ = 1.54 Å). Scans were collected at 2θ = 20−90° with a 0.05° step size.

Specific surfaces areas were obtained by N_2 adsorption measured at 77 K using the BET method on a Micromeritics ASAP 2020 automated analyzer.

Elemental analysis of the HAP catalyst was performed by Galbraith Laboratories (Knoxville, TN) using inductively coupled plasma optical emission spectroscopy (ICP-OES) for calcium and phosphorus content in the bulk material. The chemical composition on the surface of the HAP sample was analyzed by X-ray photoelectron spectroscopy (XPS) using a ThermoFisher ESCALab 250 apparatus. The signals were referenced to adventitious carbon (C(1s)) at a binding energy of 285.09 eV.

2.3. Ethanol Coupling Reactions. Guerbet coupling of ethanol was performed in a downward flow, fixed-bed, stainless steel, tubular reactor (i.d.: 0.46 cm) at 1.3 atm total system pressure. The catalyst pellets (0.2 g of MgO or 0.063 g of HAP) rested upon a packed region of quartz wool in the reactor tube with a thermocouple positioned at the center of the catalytic bed. Prior to reaction, the catalysts were heated in situ to 773 K at 10 K min^{-1} in flowing He (50 cm^3 min^{-1}) and held at 773 K for 1 h. The reactor effluent was analyzed by an online SRI 8610C gas chromatograph equipped with a flame ionization detector (FID). Reactants and products were quantified using a Restek MXT-Q-Bond column (0.53 mm i.d., 30 m length) connected to the FID.

The peak areas of reactants and products identified by GC were used to determine the ethanol conversion and selectivity of products. The conversion of ethanol was calculated as follows:

$$\text{conversion (C\%)} = \left(\frac{\Sigma n_i M_i}{2}\right) \times 100$$

where n_i is the number of carbon atoms in product i and M_i is the molar ratio of product i detected to the initial moles of ethanol.

The selectivity toward product i was calculated on the basis of the total number of carbon atoms in the product and is therefore defined as

$$\text{selectivity (C\%)} = \frac{n_i M_i}{\Sigma n_i M_i} \times 100$$

DOI: 10.1021/cs502023g
ACS Catal. 2015, 5, 1737−1746

2.4. Multiproduct SSITKA. A schematic of the reactor system used for the multiproduct SSITKA experiments is shown in Figure 1. Details regarding the system were described

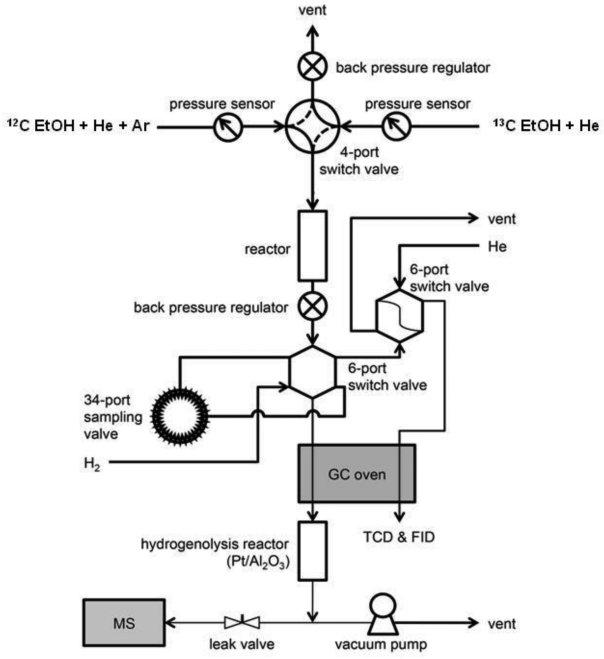

Figure 1. Reaction system for multiproduct SSITKA. This figure is adapted from Shou and Davis.[29]

in previous work from our group,[29] so only a brief description is provided here. After achieving steady-state conversion (minimum of 16 h on stream), an isotopic switch was performed using a Valco 2-postion pneumatic valve, from unlabeled ^{12}C ethanol (anhydrous, Sigma-Aldrich, 99.5%) to doubly labeled ^{13}C ethanol (Cambridge Isotopes Laboratories, Inc.; 1,2-^{13}C, 99%). The unlabeled/labeled ethanol were each contained in two identical saturators that were submerged in a heated water bath maintained at 299 K. The ^{13}C-labeled ethanol was received with a substantial amount of water (5.89 wt %); therefore, 3A molecular sieves (Sigma-Aldrich) that were previously treated at 523 K for several hours in flowing He, were added to the saturator to dehydrate the ethanol. Molecular sieves were also added to the unlabeled ethanol so that the liquid level in both saturators was the same.

Helium (GTS-Welco, 99.999%) was used as the carrier gas and flowed through the saturators with a mole fraction of ethanol in the gas phase equal to 6.2%. The ^{12}C ethanol gas feed was mixed with an inert argon (GTS-Welco, 99.999%) tracer (2 vol % of the total flow rate) that was used to correct for the gas-phase holdup in the reactor. The SSTIKA experiments were conducted at three different total gas flow rates (30, 50, and 75 cm^3 min^{-1}) to investigate reactant and product readsorption effects.

The ^{12}C/^{13}C ethanol switch was achieved without disrupting the steady-state of the reaction by maintaining the reaction temperature as well as the total system pressure at 1.3 atm, with the use of two back pressure regulators positioned at the end of the reactor and the vent line. Following the isotope switch, 16 gas samples of the reactor effluent were collected at various time intervals throughout the transient, using an automated Valco 34-port sampling valve. The samples were injected and separated by gas chromatography (GC). To avoid fragmentation and overlapping issues that are often associated with mass spectrometric (MS) analysis of higher alcohols, the gas samples were passed to a hydrogenolysis reactor held at 673 K and converted into methane over 5 wt % Pt/Al_2O_3 (Sigma-Aldrich) after separation by GC and prior to entering the MS (Pfeiffer Vacuum). In the MS, the ion signals for m/z = 15 ($^{12}CH_4$) and 17 ($^{13}CH_4$) were continuously monitored to determine the isotope content of the original gas sample. On the basis of the fragmentation pattern for methane, a portion of the $^{12}CH_4$ signal is attributed to $^{13}CH_4$; therefore, the MS $^{12}CH_4$ responses were all corrected by subtracting the $^{13}CH_4$ contribution.

Figure 2 shows an example set of normalized transient response curves for Ar, acetaldehyde, butanol, and ethanol that

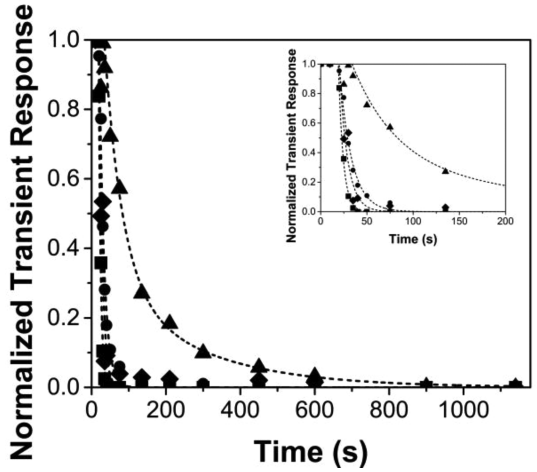

Figure 2. Normalized isotopic transient response curves following the switch from unlabeled ethanol to doubly labeled ^{13}C-labeled ethanol with a total flow of 50 cm^3 min^{-1} at 613 K during the coupling of ethanol over HAP: (■) argon, (♦) acetaldehyde, (●) ethanol, (▲) butanol.

were obtained following the isotopic switch from ^{12}C ethanol to ^{13}C ethanol during the steady-state reaction of ethanol over HAP at 613 K at a total flow rate of 50 cm^3 min^{-1}. Transient responses were normalized by the difference between the initial and final ion signals. The argon decay curve was used to determine the gas-phase holdup of the reactor system since we assumed that the inert gas did not adsorb or react on the surface of the catalyst. Therefore, the difference in area under the normalized transient response of each species (F_i) from that of the inert Ar tracer (F_{Ar}) is equal to the overall mean surface residence time associated with that species (τ_i):

$$\tau_i = \int_0^\infty (F_i - F_{Ar})\, dt$$

The surface coverage of reactant or reactive intermediates that lead to a specific product (N_i) can then be determined as follows:

$$N_i = R_i \times \tau_i$$

where R_i refers to the steady-state flow rate of reactant or the reaction rate to form product, i.

2.5. Adsorption Microcalorimetry. Adsorption sites on HAP and MgO were characterized using adsorption microcalorimetry of carbon dioxide, triethylamine (TEA), and ethanol. The experiments were conducted at 303 K using a

DOI: 10.1021/cs502023g
ACS Catal. 2015, 5, 1737−1746

heat-flow microcalorimeter. Experimental procedures[27] as well as a detailed description of the apparatus[30] used for the calorimetry measurements have been reported in previous work.

In summary, samples were first outgassed at 773 K for 16 h under vacuum to a pressure below 10^{-3} Torr then cooled to room temperature. Prior to adsorption, the pretreated sample cell was inserted into an isothermal heat block (maintained at 303 K) for 2 h and allowed to thermally equilibrate with the system. Incremental doses of the gas probe molecule (carbon dioxide, triethylamine, ethanol) were introduced to the catalyst via a volumetric dosing system. Liquid TEA and ethanol were purified by several freeze−pump−thaw cycles prior to use. Adsorption isotherms and differential enthalpies of adsorption were obtained by measuring the amount of adsorbed species on the catalytic surface and the heats evolved for each dose.

2.6. Diffuse Reflectance Infrared Fourier Transform Spectroscopy (DRIFTS). Stepwise temperature-programmed desorption (STPD) of adsorbed ethanol was investigated in the diffuse reflectance mode on a Bio-Rad (FTS-60A) FTIR spectrometer equipped with a liquid-nitrogen-cooled MCT detector. The DRIFTS experiments were conducted using a high-temperature gas reaction chamber (Harrick Scientific) positioned onto a Praying Mantis diffuse reflectance sample accessory. All spectra were obtained by coadding and averaging 100 scans at a spectral resolution of 4 cm^{-1}.

The STPD measurements were carried out according to the experimental procedure described in detail in previous work by Birky et al.[27] Catalyst samples, diluted in KBr powder at 1 wt % HAP and 5 wt % MgO, were loaded into the DRIFTS cell and pretreated in situ at 773 K for 1 h in flowing He (30 cm^3 min^{-1}). The DRIFTS cell was exposed to anhydrous ethanol (Sigma-Aldrich) at 303 K for 15 min by passing He (30 cm^3 min^{-1}) through an ethanol saturator followed by purging under He flow (30 cm^3 min^{-1}) for 15 min. The catalyst sample was then heated stepwise to 673 at 10 K min^{-1} with IR spectra collected after waiting 15 min at each temperature. The DRIFTS spectrum of the catalyst sample taken at each temperature prior to ethanol adsorption was used as background for each measurement.

3. RESULTS

3.1. Catalyst Characterization. Powder X-ray diffraction patterns of the investigated materials are shown in Figure 3. The magnesia catalyst (Figure 3a) had an XRD pattern that is characteristic of periclase MgO, the cubic form of magnesium oxide. The XRD pattern of the stoichiometric HAP material, prepared via coprecipitation (Figure 3b), confirmed that the sample was composed of crystalline hydroxyapatite and that no other phases were present.

The BET surface areas of the HAP and MgO catalysts used for this work are summarized in Table 1. Surface analysis by XPS revealed that the HAP material had a lower Ca/P surface molar ratio (1.46) than that measured in the bulk by ICP-OES (1.66). The surface deficiency in calcium is consistent with prior works and is likely due to its susceptibility to lattice substitutions and an ability to assemble in nonstoichiometric forms.[31−33]

3.2. Steady-State Conversion of Ethanol. The reactivity results obtained during the steady-state conversion of ethanol over MgO at 653 K at three different total gas flow rates are presented in Table 2. Acetaldehyde, formed via dehydrogenation of ethanol, was the primary product at low ethanol

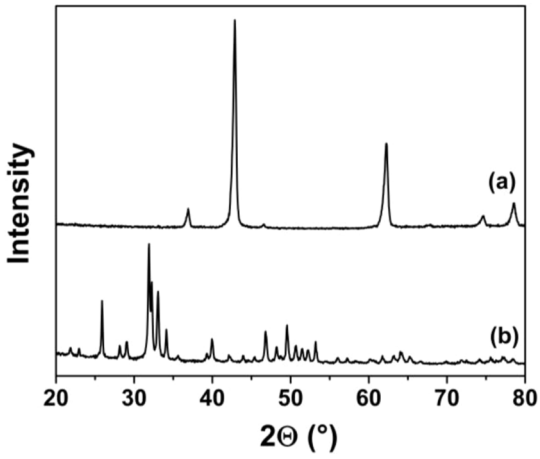

Figure 3. X-ray diffraction patterns of (a) MgO and (b) stoichiometric HAP (catalysts were calcined at 873 K for 2 h in air). Patterns are offset for clarity.

Table 1. Specific Surface Areas of Stoichiometric Hydroxyapatite and Magnesia Catalysts

catalyst	BET surface area (m^2 g^{-1})
HAP	35
MgO	35

Table 2. Product Distribution during the Catalytic Conversion of Ethanol over MgO at 653 K

			selectivity (C%)		
total flow rate (cm^3 min^{-1})	ethanol conv (%)	rate ethanol conv (mol m^{-2} s^{-1})	ethene	acetaldehyde	butanol
30	7.9	1.5×10^{-8}	11	49	40
50	4.5	1.4×10^{-8}	12	67	21
75	3.7	1.7×10^{-8}	13	67	20

Catalyst loading: 0.2 g; T = 653 K; total system pressure = 1.3 atm.

conversion (<5%). As conversion increased, the product distribution shifted toward the coupled product, butanol, as expected for a sequential reaction network in which acetaldehyde is a reaction intermediate in the conversion of ethanol into butanol. The dehydration reaction of ethanol to ethene, which is an undesired side reaction, was also observed over MgO at 653 K. The ethene selectivity remained constant (∼10%) at the reaction conditions tested. Constant ethene selectivity was also observed in previous work by Birky et al. over MgO at 673 K over a wide range of ethanol conversions (7−23%).[27]

Table 3 presents the analogous results obtained from the steady-state reaction of ethanol over stoichiometric hydroxyapatite at 613 K at three different total flow rates. Butanol was the major product observed at all three conditions, with selectivities toward the coupled product >60% even at conversions as low as 3.2%. The dehydrated side product ethene was a minor product observed during the coupling of ethanol over HAP with a selectivity of only 1% at the reaction conditions investigated. It should also be noted that the temperature of the reaction over HAP (613 K) was 40 K lower than that over MgO, and even at the lower temperature, the HAP catalyst was ∼300% more active in the ethanol coupling reaction than MgO on a surface area basis (Tables 2,3).

DOI: 10.1021/cs502023g
ACS Catal. 2015, 5, 1737−1746

Table 3. Product Distribution during the Catalytic Conversion of Ethanol over Stoichiometric HAP at 613 K

total flow rate (cm^3 min^{-1})	ethanol conv (%)	rate ethanol conv (mol m^{-2} s^{-1})	selectivity (C%) ethene	acetaldehyde	butanol
30	6.6	4.1×10^{-8}	1	24	75
50	4.3	4.4×10^{-8}	1	32	67
75	3.2	5.0×10^{-8}	1	36	63

Catalyst loading: 0.06 g; T = 613 K; total system pressure = 1.3 atm.

Ethanol conversions obtained during the steady-state Guerbet coupling of ethanol over HAP and MgO are plotted in Figure 4 as a function of inverse volumetric flow rate, which

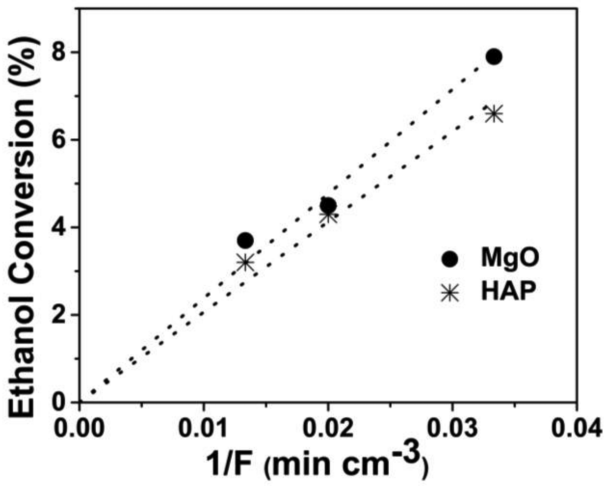

Figure 4. Conversion of ethanol as a function of inverse reactant flow rate during the coupling of ethanol over MgO and stoichiometric HAP at 653 and 613 K, respectively. The observed linear dependence confirms differential reactor conditions.

is proportional to reactor space time. Linearity of the results confirms that the reactor was operated differentially with respect to ethanol conversion.

3.3. Multiproduct SSITKA. Multiproduct SSITKA measurements during the Guerbet coupling of ethanol over MgO and HAP allowed for the quantification of important kinetic parameters of the reaction, such as surface concentrations of reaction intermediates (N_i), mean surface residence times of adsorbed species (τ), and an approximation for the intrinsic turnover frequencies of the catalyic cycle.

The average surface residence time and surface coverage of ethanol on MgO and HAP with varying flow rate are summarized in Table 4. The surface coverage of ethanol on MgO was ~5.0×10^{-6} mol m^{-2} (between 4.5 and 5.7 $\times$ 10^{-6} mol m^{-2}), regardless of total flow rate, which agrees well with results obtained previously in our lab on MgO at 673 K.[27] Significantly higher surface coverages of ethanol were observed on HAP at 613 K. Since a lower temperature and a smaller HAP sample mass loading relative to MgO were required to maintain low conversion, the interaction of ethanol with the reactor system walls and quartz wool plug would be relatively more important in the HAP experiments. A blank SSITKA experiment was thus performed at the two highest flow rates (50 and 75 cm^3 min^{-1}) to determine the surface residence time of the ethanol in the system. This time constant associated with the blank reactor was then subtracted from the measured $\tau_{ethanol}$ to give a "corrected" $\tau_{ethanol}$ associated with the catalyst at each flow rate (50 and 75 cm^3 min^{-1}), which was used to calculate a "corrected" value of ethanol surface coverage accounting for ethanol adsorption in the reactor system (Table 4). Evidently, the surface coverage of ethanol was similar on both MgO and HAP, at ~5.0×10^{-6} mol m^{-2}.

Figure 5 compares the normalized transient decays for ^{12}C-unlabeled butanol obtained over HAP with that obtained over

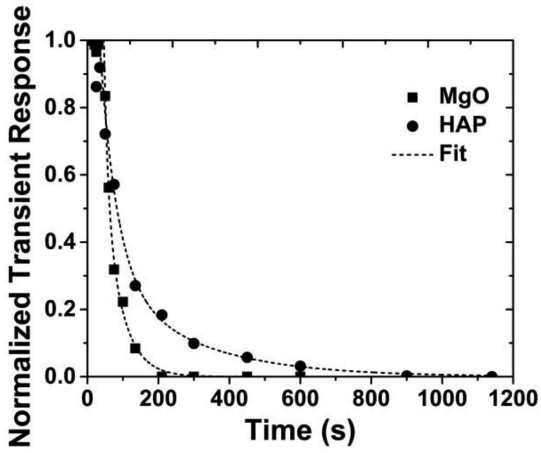

Figure 5. Normalized isotopic transient response curves for butanol following the switch from unlabeled ethanol to doubly labeled ^{13}C-labeled ethanol with a total flow of 50 cm^3 min^{-1} during the coupling of ethanol over MgO at 653 K and HAP at 613 K. Curves have been fit using a two-term exponential decay function.

MgO, during the steady-state reaction of ethanol following a switch from ^{12}C-labeled ethanol to ^{13}C-labeled ethanol. The butanol response curves presented in Figure 5 were fit with a two-term exponential decay function. The ^{12}C butanol signal observed with the HAP catalyst exhibited a slow decay that did not fully reach background level until after 900 s. The butanol transient over MgO, on the other hand, was completed after only 300 s.

Mean surface residence times as well as coverages of surface intermediates that led to acetaldehyde and butanol are summarized in Tables 5 and 6, respectively. For both MgO

Table 4. Time Constants and Surface Coverages of Ethanol ($N_{ethanol}$) during the Steady-State Guerbet Coupling of Ethanol over MgO and HAP at 653 and 613 K, Respectively

total flow rate (cm^3 min^{-1})	$\tau_{ethanol}$ (s) MgO (653 K)	HAP (613 K)	coverage of ethanol, $N_{ethanol}$ (mol m^{-2}) MgO (653 K)	HAP (613 K)	HAP (corrected) (613 K)
30	25	43	4.8×10^{-6}	2.7×10^{-5}	
50	18	8.8	5.7×10^{-6}	9.1×10^{-6}	3.9×10^{-6}
75	10	7.1	4.5×10^{-6}	1.1×10^{-5}	5.0×10^{-6}

DOI: 10.1021/cs502023g
ACS Catal. 2015, 5, 1737−1746

Table 5. Time Constants and Surface Coverages of Reactive Intermediates Leading to Acetaldehyde (N_{AcH}) during the Steady-State Guerbet Coupling of Ethanol over MgO and HAP at 653 and 613 K, Respectively

	τ_{AcH} (s)		coverage of intermediates to acetaldehyde, N_{AcH} (mol m^{-2})	
total flow rate (cm^3 min^{-1})	MgO (653 K)	HAP (613 K)	MgO (653 K)	HAP (613 K)
30	15	4.4	1.1×10^{-7}	4.3×10^{-8}
50	13	4.6	1.2×10^{-7}	6.5×10^{-8}
75	11	4.6	1.2×10^{-7}	8.2×10^{-8}

Table 6. Time Constants and Surface Coverages of Reactive Intermediates Leading to Butanol ($N_{butanol}$) during the Steady-State Guerbet Coupling of Ethanol over MgO and HAP at 653 and 613 K, Respectively

	$\tau_{butanol}$ (s)		coverage of intermediates to butanol, $N_{butanol}$ (mol m^{-2})	
total flow rate (cm^3 min^{-1})	MgO (653 K)	HAP (613 K)	MgO (653 K)	HAP (613 K)
30	93	310	2.8×10^{-7}	4.8×10^{-6}
50	53	117	8.1×10^{-8}	1.7×10^{-6}
75	27	69	4.6×10^{-8}	1.1×10^{-6}

and HAP, the average surface lifetime of reactive intermediates leading to acetaldehyde was much shorter than that leading to butanol. Stated another way, it took a significantly longer time for butanol to exit the reactor compared with acetaldehyde. The surface coverage of reaction intermediates leading to acetaldehyde relative to butanol on the two catalysts also provides valuable information. On MgO, there was a higher number of intermediates that led to acetaldehyde compared with those that led to butanol ($N_{AcH} > N_{BuOH}$), whereas the opposite trend was observed over HAP ($N_{BuOH} \gg N_{AcH}$). Moreover, Table 6 indicates the surface density of adsorbed intermediates leading to butanol was orders of magnitude greater on HAP than on MgO at all three flow rates investigated.

The readsorption of reactants or products in the reaction can have a significant influence on the time constant measured by SSITKA. The possible effect of readsorption can be seen in the variation of τ for ethanol and butanol with respect to flow rate listed in Tables 4 and 6, respectively. The mean surface residence times of adsorbed intermediates to acetaldehyde (τ_{AcH}) (Table 5), however, were relatively independent of total flow rate, which suggests acetaldehyde readsorption was negligible. Because butanol is the product of a sequential surface reaction, the contribution of readsorption to the butanol formation time constant cannot be determined by simply varying the flow rate. This concept will be explored in the Discussion section.

3.4. STPD of Adsorbed Ethanol Monitored by DRIFTS. To probe the interaction of ethanol on the catalytic surfaces, DRIFTS of preadsorbed ethanol on MgO and HAP followed by STPD was performed. The spectra obtained from these experiments are presented in Figure 6.

The left plot in Figure 6 shows IR bands observed in the 3200−2600 and 1300−1000 cm^{-1} regions after ethanol adsorption on MgO at 303 K at various temperatures. The bands are characteristic of adsorbed ethoxide species formed on the surface of the catalyst. The peaks at 2954 (υCH_3), 2917

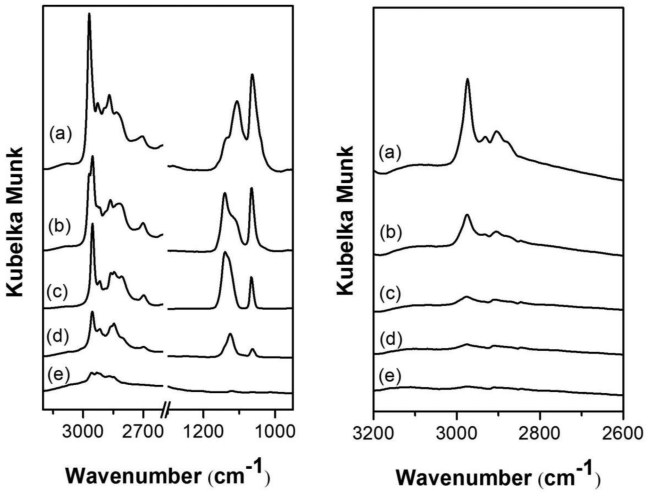

Figure 6. DRIFTS spectra of adsorbed ethanol at 303 K on MgO (left) and HAP (right) collected after heating to various temperatures: (a) 303, (b) 373, (c) 473, (d) 573, and (e) 673 K. Spectra are offset for clarity.

(υCH_3), and 2847 (υCH_2) cm^{-1} are attributed to C−H stretches of ethoxide, and the bands observed at 1125 and 1063 cm^{-1} correspond to the two C−C−O stretching modes of the adsorbed ethoxide species.[27] Features of the surface ethoxide intermediate in the C−H stretching region remain evident on the MgO surface up to 673 K.

The DRIFTS spectra collected of adsorbed ethanol on HAP at 303 K followed by stepwise heating to 673 K are displayed in Figure 6 (right). The adsorption of ethanol revealed three peaks in the 3100−2800 cm^{-1} region that can be assigned to the C−H stretches of a surface ethoxide species: 2975 (υCH_3), 2932 (υCH_2), and 2904 cm^{-1} (υCH_3). Lower wavenumber bands associated with ethoxide could not be detected because of strong absorption by the HAP material in this region. The intensity of the C−H bands attributed to ethoxide significantly decreased after heating the sample to just 373 K. Upon further heating to 573 K, the bands were not observed, indicating ethoxide had completely desorbed from HAP at this temperature. This result is consistent with previous reports on hydroxyapatite materials that also showed the disappearance of C−H ethoxide bands by 573 K.[34]

3.5. Adsorption Microcalorimetry of Carbon Dioxide, Triethylamine and Ethanol. Adsorption sites on the catalytic materials were also characterized by adsorption microcalorimetry at 303 K. The experimental results, obtained from the adsorption of carbon dioxide, triethylamine, and ethanol, are summarized in Figures 7, 8, and 9, respectively.

Carbon dioxide was used to probe the surface base properties of the catalysts. Isotherms obtained from the adsorption microcalorimetry of CO_2 on MgO and HAP are given in Figure 7. The total adsorption capacity, or uptake of each probe molecule on the catalytic surface, was determined by extrapolating the high pressure, horizontal portion of the isotherm (corresponds to saturation) to zero pressure. For CO_2 on MgO and HAP, the capacity was 1.0 and 2.5 μmol m^{-2}, respectively, suggesting a significantly higher base site density on the surface of stoichiometric hydroxyapatite compared with that observed on MgO.

Figure 7b presents the differential heats of CO_2 adsorption on MgO and HAP as a function of surface coverage. The initial differential heat of CO_2 adsorption on MgO was ~20 kJ mol^{-1}

DOI: 10.1021/cs502023g
ACS Catal. 2015, 5, 1737−1746

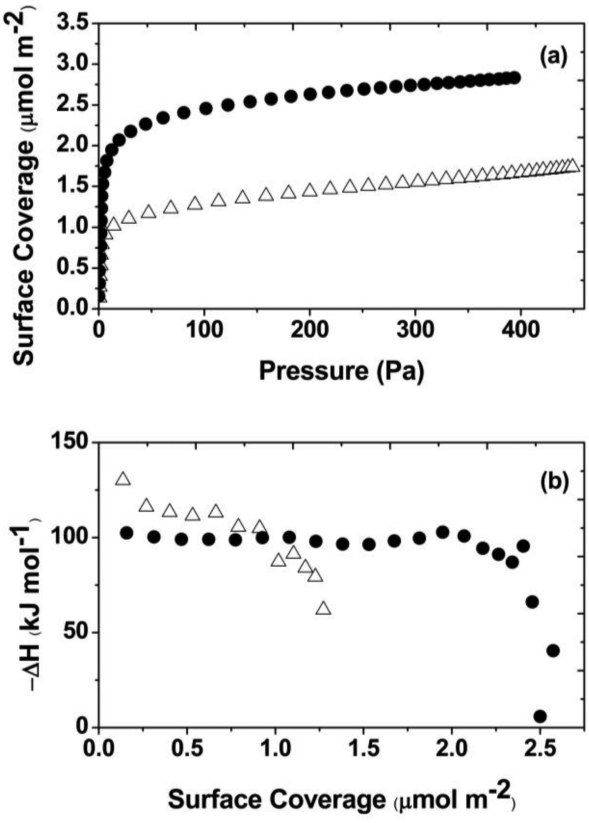

Figure 7. Adsorption microcalorimetry of carbon dioxide on (Δ) MgO and (●) stoichiometric hydroxyapatite (HAP) catalysts at 303 K; (a) adsorption isotherms of carbon dioxide and (b) differential heats of adsorption as a function of coverage.

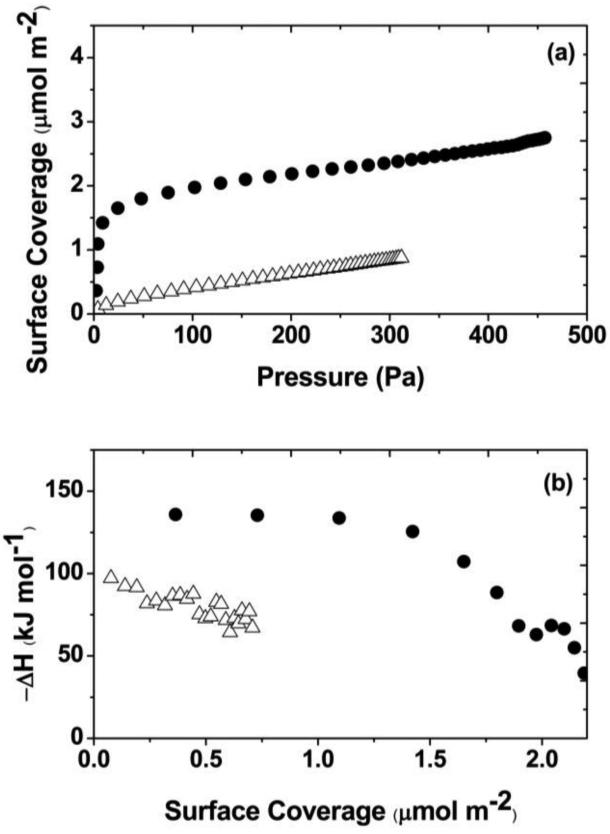

Figure 8. Adsorption microcalorimetry of triethylamine on (Δ) MgO and (●) stoichiometric hydroxyapatite catalysts at 303 K; (a) adsorption isotherms of triethylamine and (b) differential heats of adsorption as a function of coverage.

higher than that on HAP, which implies MgO exposes stronger base sites that interact with CO_2 compared with those on HAP.

Adsorption microcalorimetry of ammonia has been employed extensively as a probe of surface acidity; however, there can be multiple interactions with ammonia and solid surfaces. These additional adsorption states include weak hydrogen bonding interactions with the surface as well as deprotonation of ammonia by strong base sites to form surface NH_2 species.[35]

Triethylamine (TEA) is harder to deprotonate and is therefore less susceptible to dissociation on the surface. It also has a stronger proton affinity than ammonia, suggesting it is a stronger gas-phase base and should therefore be more selective in probing surface acid sites.[36]

Adsorption isotherms of TEA obtained on MgO and HAP at 303 K are presented in Figure 8a. The low observed uptake and linear variation of TEA surface coverage with pressure on MgO indicate a very weak interaction with the surface. In contrast, TEA was chemisorbed onto the HAP catalytic surface with an overall uptake of 1.7 μmol m^{-2}, which is illustrated by its Langmuirian adsorption isotherm. A weak surface interaction between TEA and MgO is confirmed by the relatively low differential heats of TEA adsorption on MgO compared with those observed on HAP (Figure 8b). Evidently, HAP exposes a considerably higher acid site density than MgO.

Figure 9 shows the results from adsorption microcalorimetry of ethanol on MgO and HAP at 303 K. The adsorption isotherms for the two catalysts in Figure 9a were nearly identical, resulting in an overall ethanol uptake of 5.1 μmol m^{-2} on MgO and 5.2 μmol m^{-2} on HAP. These results are consistent with the surface coverages of ethanol on MgO and HAP determined by SSITKA (Table 4).

Differential heats of ethanol adsorption as a function of surface coverage for the catalysts are provided in Figure 9b. The initial differential heats observed on MgO and HAP were ~118 and ~90 kJ mol^{-1}, respectively. This ~30 kJ mol^{-1} difference in adsorption energy suggests that the ethanol interacts more weakly with HAP compared with MgO, which is consistent with the results obtained from STPD of preadsorbed ethanol (Figure 6) that reveal desorption of ethanol from HAP at a significantly lower temperature than from MgO. It is also worth mentioning that the ethanol adsorption sites on both MgO and HAP appear to be fairly uniform in strength, indicated by the invariance in ΔH_{ads} as a function of coverage up to about 4 μmol m^{-2} (Figure 9b).

4. DISCUSSION

The SSITKA measurements allowed for the direct quantification of critical kinetic parameters, such as mean surface residence times, as well as surface coverages of intermediates leading to products formed in the reaction. Transient results revealed that for both MgO and HAP, the residence time for intermediates leading to acetaldehyde (τ_{AcH}) was much shorter than the residence time of reaction intermediates leading to butanol (τ_{BuOH}) at all three flow rates investigated. Moreover, the residence times of ethanol and butanol depended strongly on flow rate, which suggests that the alcohols readsorbed and desorbed as they passed through the reactor. It is tempting to extrapolate the SSITKA results to infinite flow rate in an

DOI: 10.1021/cs502023g
ACS Catal. 2015, 5, 1737−1746

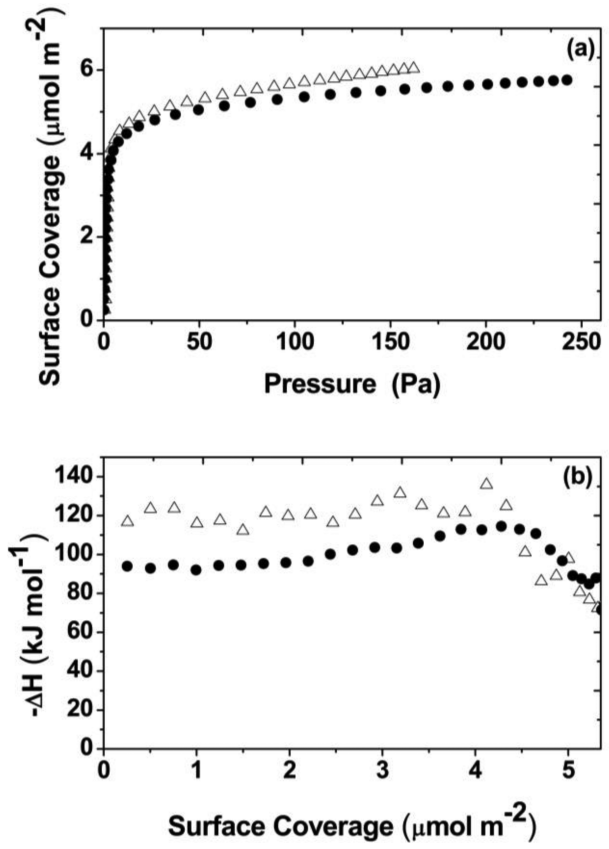

Figure 9. Adsorption microcalorimetry of ethanol on (Δ) MgO and (●) stoichiometric hydroxyapatite (HAP) catalysts at 303 K; (a) adsorption isotherms of ethanol and (b) differential heats of adsorption as a function of coverage.

attempt to remove the effects of readsorption on the calculated time constants. Unfortunately, the selectivity to butanol during Guerbet coupling can depend on ethanol conversion because of the sequential nature of the reaction network to produce butanol. Therefore, the discussion of SSITKA results will be focused on those determined at the highest flow rate, 75 cm^3 min^{-1}, which is a compromise between achieving a measurable conversion level and minimizing readsorption effects. From Table 4, the values of $\tau_{ethanol}$ for MgO and HAP were 10 and 7.1 s, respectively, and provide a reasonable estimation of the time constant for an alcohol to desorb from the catalyst bed and exit the reactor. The values of $\tau_{butanol}$ reported in Table 6 for MgO and HAP were 27 and 69 s, respectively, at 75 cm^3 min^{-1} total flow rate. The substantially longer time constants associated with butanol formation compared with ethanol desorption over both materials suggests that the butanol time constants are determined primarily by reaction kinetics instead of adsorption/desorption artifacts. Moreover, since the ratio of ethanol to butanol in the gas phase at the reactor exit is >50:1 over both catalysts, the competitive adsorption of ethanol over butanol should also help to minimize readsorption effects in the time constant associated with butanol formation.

A commonly hypothesized reaction path for the Guerbet coupling of ethanol involves the aldol condensation of intermediate acetaldehyde, which likely proceeds through a surface enolate species that produces coupled products that desorb as butanol. In this coupling path, surface acetaldehyde produced from ethanol dehydrogenation may desorb or undergo base-catalyzed abstraction of the α-H to form an adsorbed enolate species. The isotopic transient results obtained during the steady-state conversion of ethanol over MgO revealed a significantly higher surface coverage of reactive intermediates leading to acetaldehyde than to butanol (Tables 5, 6: $N_{AcH} > N_{BuoH}$) at all flow rates. These results suggest a higher fraction of surface acetaldehyde produced during the reaction of ethanol on MgO desorbed rather than coupled form butanol. The coverages N_{AcH} and N_{BuOH} are consistent with the higher selectivity to acetaldehyde compared with butanol observed over MgO.

In contrast, the coverage of intermediates that led to butanol on HAP was higher than that leading to acetaldehyde by roughly 1−2 orders of magnitude ($N_{BuOH} \gg N_{AcH}$), regardless of flow rate (Tables 5, 6). Evidently, the majority of acetaldehyde formed from ethanol dehydrogenation on HAP remained on the surface to undergo sequential reactions leading to butanol formation.

A previous study from our group on ethanol coupling over MgO investigated the relationship between butanol rate and acetaldehyde concentration over a broad range of ethanol conversions (7−23%) and observed a first-order dependence of butanol formation on gas-phase acetaldehyde concentration.[27] In the current work on MgO, a 36% decrease in gas-phase acetaldehyde concentration at the reactor exit (from 57.8 μmol L^{-1} to 37.2 μmol L^{-1} at 7.9% and 3.7% ethanol conversion, respectively) corresponded to a 44% decrease in butanol production rate (3.0×10^{-9} to 1.7×10^{-9} mol s^{-1} m^{-2}), which is consistent with earlier work and confirms a strong dependence of butanol formation on acetaldehyde concentration. Interestingly, a 28% decrease in gas-phase acetaldehyde concentration at the reactor exit during ethanol coupling over HAP was not accompanied by a significant change in the production rate of butanol. These results suggest that most of the butanol formed over HAP did not involve the participation of gas-phase acetaldehyde, whereas the butanol formation over MgO might involve a surface that is closer to equilibrated with gas-phase acetaldehyde.

Adsorption microcalorimetry of CO_2 was performed to investigate the number and nature of base sites on the catalytic surfaces. Microcalorimetry results revealed that the coverage of CO_2 on the HAP surface was 2.5 times that of MgO. However, differential heats of CO_2 adsorption on HAP were lower than on MgO. Recent IR studies on HAP have shown that CO_2 interacts with the OH^- groups and the O^{2-} atoms of surface PO_4^{3-} groups.[37] Adsorption microcalorimetry suggests that relative to MgO, HAP exposed a higher number density of base sites but that the sites were weaker in adsorption binding energy. Adsorption microcalorimetry of TEA also revealed a higher acid site density on the surface of HAP compared with MgO. Since the Guerbet coupling of ethanol likely occurs on acid−base site pairs, the high reactivity of ethanol on HAP compared with MgO appears to be related to high number of acid−base site pairs with appropriate binding affinity on HAP. The higher density of these preferred site pairs may also explain why a significantly higher surface coverage of intermediates leading to butanol was observed on HAP relative to MgO.

Stepwise temperature-programmed desorption of preadsorbed ethanol at 303 K on MgO and HAP was studied using DRIFTS. The IR spectra revealed the formation of a surface ethoxide intermediate on both of the catalytic materials. Ethanol dissociatively adsorbs on the surface forming ethoxide coordinated to a Lewis acid site (Ca^{2+} on HAP, Mg^{2+} for MgO) and proton-like hydrogen coordinated to a Brønsted base site.

DOI: 10.1021/cs502023g
ACS Catal. 2015, 5, 1737−1746

The STPD results show that the ethoxide species on HAP mostly desorbed from the surface by 473 K, whereas a temperature of 673 K was required on MgO. This 200 K difference in desorption temperature indicates that the dissociated ethanol is much more weakly held to HAP relative to MgO, which is consistent with the results obtained from adsorption microcalorimetry of ethanol where the initial differential heat of ethanol adsorption on HAP was ∼30 kJ mol^{-1} lower than that on MgO.

The TOF based on ethanol adsorption is a lower bound because not all of the adsorbed ethanol proceeds to product. A better estimate of the TOF can be derived from the isotopic transient results as the reciprocal of the mean surface residence time (TOF = τ^{-1}). Unfortunately, the readsorption of alcohols during the transient increased the measured surface residence time. If we try to minimize the effects of readsorption by using the surface residence time of intermediates to butanol at the highest flow rate in the study (75 cm^3 min^{-1}), we have τ_{BuOH} = 27 and 69 s for MgO (653 K) and HAP (613 K), respectively. Moreover, if we assume that the τ_{EtOH} at high flow rate is a reasonable approximation of the effect of readsorption, then we can simply subtract the value for τ_{EtOH} (Table 4) from τ_{BuOH} (Table 6), as reported by Birky et al. to get a "corrected" τ_{BuOH}. The inverse of the "corrected" τ_{BuOH} provides a better estimate of the TOF associated with intermediates that form butanol, denoted as TOF_{SSITKA}. The values derived from Tables 4 and 6 are 0.059 s^{-1} for MgO (653 K) and 0.016 s^{-1} for HAP (613 K). The values of TOF_{SSITKA} for acetaldehyde production can be estimated as the inverse of the τ_{AcH} at the highest flow rate because readsorption appears to be insignificant; thus, the TOF_{SSITKA} for AcH is 0.091 s^{-1} for MgO at 653 K and 0.22 s^{-1} for HAP at 613 K. The higher selectivity to butanol over HAP compared with MgO is apparently the consequence of a much higher coverage of surface intermediates leading to butanol during the steady-state reaction.

Ogo et al.[38] used isotopic exchange reactions to show that ethanol dehydrogenation occurs rapidly on strontium-substituted hydroxyapatite catalysts and that aldol condensation is the rate-determining step. The very short residence time of intermediates leading to acetaldehyde (τ_{AcH}) relative to τ_{BuOH} observed here by SSITKA would support their kinetic mechanism. It is possible that the kinetically relevant step of the reaction is related to enolate formation via α-H abstraction of adsorbed acetaldehyde. Results from adsorption microcalorimetry of CO_2 (a general probe of base sites) and STPD of adsorbed ethanol suggest HAP has a weaker surface affinity than MgO for those probe molecules. Furthermore, adsorption of triethylamine revealed the presence of weak Lewis acid sites on HAP that were not found on MgO. Thus, under steady-state reaction conditions, more surface acid−base pairs on HAP may be available for enolate formation compared with MgO, which would lead to a higher formation rate of coupled products.

5. CONCLUSIONS

Isotopic transient studies were performed during the steady-state Guerbet coupling of ethanol to butanol over stoichiometric hydroxyapatite and MgO at 613 and 653 K, respectively. The HAP catalyst was ∼3 times more active in the reaction than MgO on a surface area basis, even at the lower TOF. The selectivity over HAP was as high as 75% to butanol.

The surface coverage of reactive intermediates leading to butanol (N_{BuOH}) relative to that leading to acetaldehyde (N_{AcH}) was very high on HAP ($N_{BuOH} \gg N_{AcH}$), whereas on MgO, $N_{AcH} > N_{BuOH}$. Given the generally accepted mechanism for Guerbet coupling that involves aldol condensation of acetaldehyde, it appears that a greater fraction of the acetaldehyde produced during the reaction proceeds toward coupling products on HAP relative to MgO.

Adsorption microcalorimetry of CO_2 showed a higher surface density of base sites on HAP compared with that on MgO, but the CO_2 adsorption binding energy was weaker on HAP. Moreover, adsorption of triethylamine revealed significant Lewis acidity on HAP and negligible acidity on MgO.

It is likely that the high activity and selectivity observed during the Guerbet coupling of ethanol over HAP involves the proper balance of acid−base site pairs to facilitate all of the steps in the sequence, including alcohol dehydrogenation, aldol condensation and aldehyde hydrogenation. The relatively strong basicity of MgO retains adsorbed ethanol at higher temperatures compared with HAP, which is consistent with the idea that Guerbet coupling is facilitated by weak acid−base bifunctional catalysts.

■ ASSOCIATED CONTENT

Supporting Information

The following file is available free of charge on the ACS Publications website at DOI: 10.1021/cs502023g.

Normalized transient response curves are provided from additional SSITKA experiments that were conducted at various flow rates (PDF)

■ AUTHOR INFORMATION

Corresponding Author

*E-mail: rjd4f@virginia.edu.

Present Address

[†](For H.S.) SABIC Technology Center, 1600 Industrial Blvd., Sugar Land, TX 77478, USA

Notes

The authors declare no competing financial interest.

■ ACKNOWLEDGMENTS

This work was supported by the Chemical Sciences, Geosciences and Biosciences Division, Office of Basic Energy Sciences, Office of Science, U.S. Department of Energy, Grant No. DE-FG02-95ER14549. The authors thank Dmitry Pestov at Virginia Commonwealth University for assistance with XPS.

■ REFERENCES

(1) Dowson, G. R. M.; Haddow, M. F.; Lee, J.; Wingad, R. L.; Wass, D. F. *Angew. Chem., Int. Ed.* **2013**, *52*, 9005−9008.
(2) Savage, N. *Nature* **2011**, *474*, S9−S11.
(3) Tsuchida, T.; Sakuma, S.; Takeguchi, T.; Ueda, W. *Ind. Eng. Chem. Res.* **2006**, *45*, 8634−8642.
(4) Koda, K.; Matsu-ura, T.; Obora, Y.; Ishii, Y. *Chem. Lett.* **2009**, *38*, 838−839.
(5) O'Lenick, A. J. *J. Surfact. Deterg.* **2001**, *4*, 311−315.
(6) Carlini, C.; Di Girolamo, M.; Macinai, A.; Marchionna, M.; Noviello, M.; Raspolli Galletti, A. M.; Sbrana, G. *J. Mol. Catal. A: Chem.* **2003**, *200*, 137−146.
(7) Veibel, S.; Nielsen, J. *Tetrahedron* **1967**, *213*, 1723−1733.
(8) Yang, C.; Meng, Z. Y. *J. Catal.* **1993**, *142*, 37−44.
(9) Ndou, A. S.; Plint, N.; Coville, N. J. *Appl. Catal. A* **2003**, *251*, 337−345.
(10) Gines, M. J. L.; Iglesia, E. *J. Catal.* **1998**, *176*, 155−172.
(11) Scalbert, J.; Thibault-Starzyk, F.; Jacquot, R.; Morvan, D.; Meunier, F. *J. Catal.* **2014**, *311*, 28−32.

DOI: 10.1021/cs502023g
ACS Catal. 2015, 5, 1737−1746

(12) Kozlowski, J. T.; Davis, R. J. *ACS Catal.* **2013**, *3*, 1588−1600.
(13) Ueda, W.; Kuwabara, T.; Ohshida, T.; Morikawa, Y. *J. Chem. Soc., Chem. Commun.* **1990**, 1558−1559.
(14) Ueda, W.; Ohshida, T.; Kuwabara, T.; Morikawa, Y. *Catal. Lett.* **1992**, *12*, 97−104.
(15) Di Cosimo, J.; Apesteguía, C.; Ginés, M.; Iglesia, E. *J. Catal.* **2000**, *190*, 261−275.
(16) León, M.; Díaz, E.; Ordóñez, S. *Catal. Today* **2011**, *164*, 436−442.
(17) Gotoh, K.; Nakamura, S.; Mori, T.; Morikawa, Y. *Stud. Surf. Sci. Catal.* **2000**, *130*, 2669−2674.
(18) Tsuchida, T.; Kubo, J.; Yoshioka, T.; Sakuma, S.; Takeguchi, T.; Ueda, W. *J. Catal.* **2008**, *259*, 183−189.
(19) Ogo, S.; Onda, A.; Yanagisawa, K. *Appl. Catal. A* **2011**, *402*, 188−195.
(20) Kibby, C. L.; Hall, W. K. *J. Catal.* **1973**, *29*, 144−159.
(21) Joris, S. J.; Amberg, C. H. *J. Phys. Chem.* **1971**, *76*, 3167−3171.
(22) Bett, J. A. S.; Christner, L. G.; Hall, W. K. *J. Am. Chem. Soc.* **1967**, *486*, 5535−5541.
(23) McClaine, B. C.; Davis, R. J. *J. Catal.* **2002**, *211*, 379−386.
(24) Gao, J.; Mo, X.; Goodwin, J. G. *J. Catal.* **2010**, *275*, 211−217.
(25) Ledesma, C.; Yang, J.; Chen, D.; Holmen, A. *ACS Catal.* **2014**, *4*, 4527−4547.
(26) Shannon, S. L.; Goodwin, J. G. *Chem. Rev.* **1995**, *95*, 677−695.
(27) Birky, T. W.; Kozlowski, J. T.; Davis, R. J. *J. Catal.* **2013**, *298*, 130−137.
(28) Tsuchida, T.; Kubo, J.; Yoshioka, T.; Sakuma, S.; Takeguchi, T.; Ueda, W. *J. Japan Pet. Inst.* **2009**, *52*, 51−59.
(29) Shou, H.; Davis, R. J. *J. Catal.* **2013**, *306*, 91−99.
(30) Bordawekar, S.; Doskocil, E.; Davis, R. *Langmuir* **1998**, *14*, 1734−1738.
(31) Stošić, D.; Bennici, S.; Sirotin, S.; Calais, C.; Couturier, J.-L.; Dubois, J.-L.; Travert, A.; Auroux, A. *Appl. Catal. A* **2012**, *447*, 124−134.
(32) Tsuchida, T.; Kubo, J.; Yoshioka, T.; Sakuma, S.; Takeguchi, T.; Ueda, W. *J. Catal.* **2008**, *259*, 183−189.
(33) Tanaka, H.; Watanabe, T.; Chikazawa, M. *J. Chem. Soc. Faraday Trans.* **1997**, *93*, 4377−4381.
(34) Faria, R. M. B.; Cesar, D. V.; Salim, V. M. M. *Catal. Today* **2008**, *133−135*, 168−173.
(35) Auroux, A.; Gervasini, A. *J. Phys. Chem.* **1990**, *94*, 6371−6379.
(36) Cardona-Martinez, N. C.; Dumesic, J. A. *Adv. Catal.* **1992**, *38*, 149−244.
(37) Diallo-Garcia, S.; Ben Osman, M.; Krafft, J.-M.; Casale, S.; Thomas, C.; Kubo, J.; Costentin, G. *J. Phys. Chem. C* **2014**, *118*, 12744−12757.
(38) Ogo, S.; Onda, A.; Iwasa, Y.; Hara, K.; Fukuoka, A.; Yanagisawa, K. *J. Catal.* **2012**, *296*, 24−30.

DOI: 10.1021/cs502023g
ACS Catal. 2015, 5, 1737−1746